energies

MDPI

Article

CFD-Based Investigation of the Operation Process of Radial Labyrinth Machinery Under Different Geometrical Configurations

Przemyslaw Szulc * and Janusz Skrzypacz

Faculty of Mechanical and Power Engineering, Department of Energy Conversion Engineering, Wroclaw University of Science and Technology, 50-370 Wroclaw, Poland; janusz.skrzypacz@pwr.edu.pl
* Correspondence: przemyslaw.szulc@pwr.edu.pl

Abstract: This study explores the performance and flow characteristics of radial labyrinth pumps (RLPs) under various geometrical configurations and operating conditions. Experimental investigations and numerical simulations were conducted to evaluate the impact of design parameters such as blade geometry, channel width and blade angle on pump hydraulic performance. The numerical model, developed using the realizable k-ε turbulence model, was validated with experimental data, achieving satisfactory convergence (4.8%—bladed active disc operating with a smooth passive disc and 3.0%—bladed active disc operating with a bladed passive disc). Analysis of the velocity profiles and vortex structures formed between the active and passive discs was performed. These findings underscore the importance of optimizing disc geometry to balance centrifugal effects and momentum exchange. The obtained head for the model with a bladed active disc operating with a smooth passive disc was H = 24.1 m, while, for the bladed active disc operating with a bladed passive disc, it was almost 1.7 times higher at H = 40.3 m. Additionally, the research identifies potential zones within the pump where energy transfer processes differ, providing insight into targeted design improvements. The findings provide valuable information on the optimization of RLP designs and their broader applicability.

Keywords: radial labyrinth machinery; low specific speed; circulation

check for updates

Citation: Szulc, P.; Skrzypacz, J. CFD-Based Investigation of the Operation Process of Radial Labyrinth Machinery Under Different Geometrical Configurations. *Energies* **2024**, *17*, 6477. https://doi.org/10.3390/en17246477

Academic Editors: Zdeněk Jegla and Tomáš Juřena

Received: 2 December 2024
Revised: 18 December 2024
Accepted: 18 December 2024
Published: 23 December 2024

Copyright: © 2024 by the authors. Licensee MDPI, Basel, Switzerland. This article is an open access article distributed under the terms and conditions of the Creative Commons Attribution (CC BY) license (https://creativecommons.org/licenses/by/4.0/).

1. Introduction

The chemical industry often requires pump systems capable of delivering high head at low flow rates, as these conditions are critical for certain chemical reactions. These requirements correspond to pumps with a low specific speed (n_q) ratio. However, commonly used centrifugal pumps designed for such operating conditions experience significant inertial losses, which result in lower efficiency. Additionally, the efficiency of these pumps tends to decrease further as the specific speed (n_q) is reduced. The limit value of the specific speed parameter (n_q) is commonly recognized as 10, primarily due to economic considerations related to the use of centrifugal pumps [1]. In many cases, specific operational requirements make centrifugal pumps the only solution. These demands have driven the development of unconventional pump designs. Examples of such innovations, documented in patent databases [2–5] and the literature, include straight radial impellers [6–8] and perforated and pipe impellers [9,10]. In such cases, labyrinth pumps, as an example of labyrinth machinery, patented first by I. A. Golubev in 1960 [11], can find applications.

Figure 1 presents conceptual views of the labyrinth machine (pump or seals) with axial (a) and radial (b) flow configurations. The increase in the energy of the pumped liquid is achieved through the interaction of moving working elements with stationary ones. For axial flow machines, a screw (2) rotates within a stationary sleeve (1) along the main axis of the unit. In contrast, for radial flow machines, a rotating active disc (4) works in conjunction with a stationary passive disc (3).

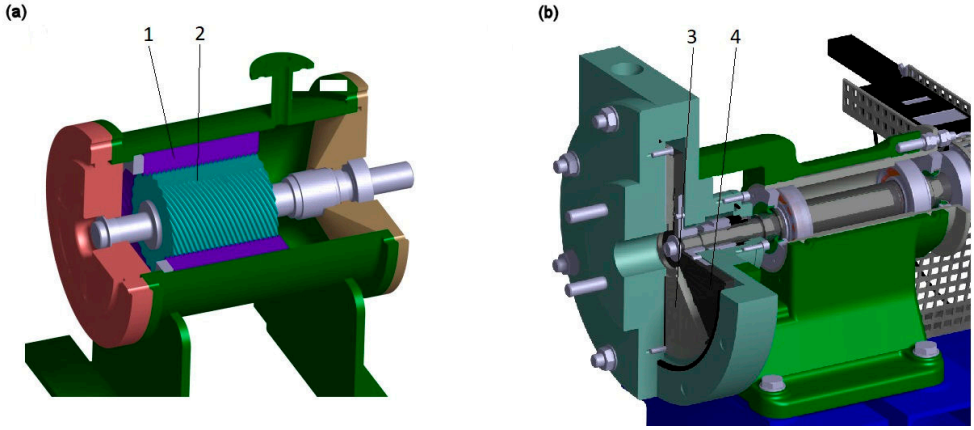


Figure 1. Labyrinth machines. (**a**) Axial flow configuration and (**b**) radial flow configuration, where 1—sleeve, 2—screw, 3—passive disc, and 4—active disc.

A distinguishing feature of these interacting working elements is the high number of grooves or blades with opposing inclination angles (if the blades or grooves on the moving element are oriented to the right, those on the stationary element are oriented to the left). In axial pumps, this is implemented as a multithreaded screw on the rotating screw and the stationary sleeve. For radial pumps, due to the increase in circumference with the radius, discs can be equipped with blades or grooves. The operation of an axial labyrinth pump, called labyrinth screw pumps, is presented in [12–15]. The authors mentioned that the performance of the pump depends on the transfer of momentum during the interaction of the fluid with both the stationary and rotating components of the pump. Within the cross-section defined by the grooves of the stationary and rotating components, vortex structures are formed, transferring momentum from the active to the passive side. This dynamic interaction results in an increase in the total head of the machine (pump).

The theory, initially proposed in [12] and further developed in [13,14,16–27], aligns the theoretical curves with a real performance by incorporating the head coefficient k. This coefficient is influenced by several factors, including thread geometry (height, width, pitch, and angle between the threads of the sleeve and cylinder); clearance between these elements; Reynolds number; and properties of the pumped fluid. Due to the complexity and number of these parameters, determining the value of k is feasible only through experimental methods [11,13,14,16,17]. Using k enables the calculation of pump characteristic curves with a convergence to real-world data within 10%. Several researchers have investigated how groove design parameters affect pump performance [28–30]. The study presented in [21] concluded that rectangular labyrinth pumps are particularly suitable for multiphase and highly viscous flows. Other studies [25,31,32] have examined structural optimization instead of focusing solely on fluid parameters. The authors in [24,33,34] developed a new approach to the calculation of labyrinth screw pumps, which incorporated the influence of the shape of the screw groove on the flow characteristics (the performance of the pump Q, P increases by up to 10%). This method has claimed to be more precise than the existing models, providing improved accuracy in predicting pump performance. Prandtl's mixing theory for Reynolds stress equations of two dimensions was utilized in [22], introducing as a new approach for the calculation of pump performance the cell head coefficient and the total pump head coefficient. This theory aligned well with the experimental findings of Golubiev. Recent studies have focused on analyzing leakage flow rates and tooth clearance pressure labyrinth seals, providing deeper insights into their hydraulic behavior, and performance optimization was presented in [35,36]. In summary, the flow mechanism in axial labyrinth machines is highly complex due to its turbulent and three-dimensional nature, dominated by the nonlinear characteristics of the governing equations. This complexity makes accurate modeling of flow behavior particularly challenging.

The first attempts at numerical modeling of flow in labyrinth seals (LS) were presented in 1980 in [37]. In [38], the hydraulic performance of three helical groove seals using CFD was examined. The authors identified the critical influence of groove width and depth, as well as helix angle, on leakage. Further works [39–41] confirmed the feasibility of using numerical methods to analyze labyrinth seals, validated by experimental results. They focused on refining the optimization of the helix angles and the design of second-stage helical groove seals.

Labyrinth screw pump (LSP) simulations have yielded valuable insights into their design and performance. The numerical modeling validation was performed in [21,42,43], where the results of rectangular labyrinth pumps were compared with those obtained from the CFD analysis. The convergence of the simulation results with the experimental data is satisfactory. The authors in [29] explored three novel LSP designs using CFD methods. They concluded that sectioning of the rotor and stator components can optimize the pump performance. The renormalization group k–ε two-equation turbulence model (RNG k–ε model) and the semi-implicit method for the pressure-linked equations-consistent algorithm, along with the Fluent CFD code, were adopted for the simulations. In [21], it was numerically demonstrated that the clearance between the screw and the sleeve has a significant impact on pump performance, which is consistent with the findings related to labyrinth seals. The k–ω SST (shear stress transport) was used. Optimization of the structural parameters of the stator and rotor was carried out in [32]. The CFD methods were applied. According to the authors, the SST (shear stress transport) k–ω turbulence model was used due to its high precision and stability. The high-viscosity fluids were analyzed in the study. It was confirmed in [44] that groove seal geometry greatly influences internal leakage, directly affecting the performance of helical grooved pumps. The k–ε turbulence models were used, and the "frozen rotor" interface model, a rotor interface treatment technique, was applied for the simulations. This approach seems inappropriate, because the clearance value is as small as 0.2 mm, which may not accurately represent the physical conditions and could lead to incorrect simulation results. In [45], the performance of the labyrinth pump was studied, both experimentally and numerically. This research demonstrated that LSPs are more effective than ESPs for handling highly viscous fluids. The applicability of the affinity law to LSPs was verified. Based on the results, dimensionless flow and head coefficients were correlated using a nonlinear relationship. The CFD analysis could be found in [46], where the authors examined the performance of pumping high-viscosity fluids. A water–glycerin mixture was used. The Reynolds-Averaged Navier–Stokes (RANS) equations, coupled with the standard SST (shear stress transport) turbulence model, were solved using a commercial CFD code. The good agreement between the numerical results and the experimental data validated the methodology adopted in this study.

The literature provides a wealth of information on CFD numerical modeling of flow passages in centrifugal pumps. Due to the nature of RLM, some of these approaches can be applied in their simulations. Recently, the works [47,48] have attracted attention. In article [47], the authors conducted cavitation modeling considering thermodynamic effects of pumps operating with cryogenic liquids. The focus of the CFD analysis was on the inducer. The SST k–ω model was used. The authors claimed that the thermodynamic effect has a great influence on the cryogenic cavitation of the inducer. To determine the actual flow field distribution and external characteristics of the pump, a coupled analysis was performed using a standard CFX simulation integrated with MATLAB [48]. The findings revealed that hub leakage enhances tip leakage and alters the main flow field distribution. The results of the internal flow model numerical simulation are closely aligned with the experimental data, with a maximum head error of 0.3 m and an efficiency error of 1.7%. Unfortunately, a detailed approach to the development of the numerical model was not provided. The key technologies and development trends of soft abrasive flow finishing investigation were presented in [49]. It briefly discusses multiphase fluid dynamics modeling, material removal mechanisms, auxiliary strengthening finishing techniques, and the observation of surface effects caused by abrasive particles and cavitation bubbles.

A brief review of the literature on labyrinth pumps reveals that research has predominantly focused on axial units, highlighting the need for a thorough investigation of radial pumps. The analysis of these pumps from a hydraulic perspective must be considered, especially in terms of flow structure, vortex generation, or performance. The numerical model, its structure and form must also be defined, as the literature does not provide precise guidelines. The approach used to model axial flow machines cannot be fully applied here. The literature review highlights that various approaches are employed for modeling axial machines, utilizing different turbulence models and geometric simplifications, which lead to diverse outcomes. This variability underscores the need for clarification when adapting these methodologies to radial pumps, emphasizing the importance of further research in this area.

This study investigates the performance and flow structure of radial labyrinth machinery (RLM) across various geometrical designs and operating modes, such as pumps or seals. The analysis highlights the pivotal role of vortex structures, formed between active and passive discs, in energy transfer and momentum exchange, which significantly affect the performance of pumps and seals. Optimized blade geometry and channel dimensions were shown to enhance vortex formation, boosting energy transfer and improving the overall performance. On the contrary, poorly designed configurations resulted in lower hydraulic efficiency and greater energy losses.

2. The Object of the Research

The radial labyrinth pump (RLP) introduces a novel approach for pumps, akin to that seen in axial units. It consists of two primary components: a stationary passive disc and a rotating active disc (terminology introduced by the author). Both discs are designed with specially designed grooves or blades (in the opposite direction for both discs). The interaction between the discs, separated by a clearance δ, enhances the overall energy of the fluid flow. More information and preliminary research on such pump are presented in [50].

As an example for considerations regarding the operation of a radial labyrinth pump, five disc sets were selected. These sets were chosen based on a review of the literature on pumps with axial flow characteristics, supplemented by conclusions drawn from the author's own research. The literature review and preliminary studies conducted by the authors enabled the identification of the following key parameters defining the geometry of the operating disc: outer diameter d_{2ap}, inlet, blade angle β, number of blades z, blade height h and its thickness s. In Table 1, the geometric parameters of the analyzed sets are presented. The geometric dimensions of the discs were selected on the basis of dimensional analysis and design of experiments (DOE).

Table 1. The parameters of the sets for the investigations.

Symbol	Number of Blades	Thickness of Blades	Angle of Blades	Hight of Blades	Inlet Diameter of Discs
	z (pcs.)	s (mm)	β_1 (°)	h (mm)	d_1 (mm)
zl0	20	2.0	30.0	4.0	120.0
zl1	20	2.0	30.0	4.0	120.0
zl2	40	4.0	50.0	4.0	120.0
zl3	20	4.0	50.0	4.0	160.0
zl4	40	2.0	30.0	2.0	120.0

The active disc of the set *zl0* was identical to *zl1*, but the passive disc was used as the smooth one. For all sets, the clearance between the discs was kept constant at δ = 0.6 mm. Additionally, an identical outer diameter of d_{2ap} = 200 mm was assumed. The shape of the blade was assumed to be curvilinear, made in the form of a logarithmic spiral with a constant angle.

The shape of the tested discs, as well as the selected geometric parameters, is shown in Figure 2. To simplify the model, it was assumed that the geometry of the active disc was identical to that of the passive disc.

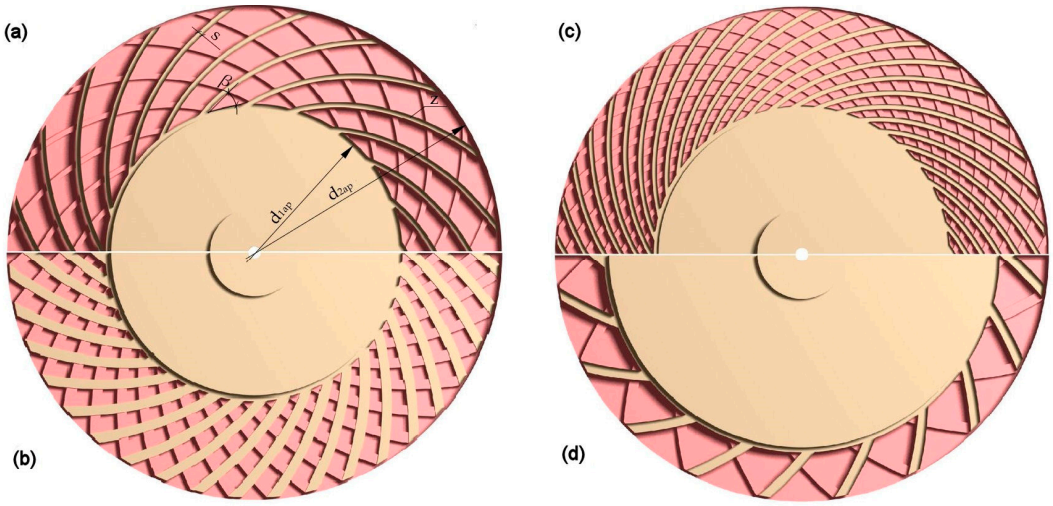


Figure 2. Geometries of the analyzed discs, sets (**a**) *zl1*, (**b**) *zl2*, (**c**) *zl3*, and (**d**) *zl4*.

3. Development of the Numerical Model for the Radial Labyrinth Pump

3.1. Assumptions of the Numerical Model

During the numerical modeling CFD, it was assumed that the flow in the pump is periodically symmetric and that each flow channel operates in the same way. For this reason, the machine model analyzed was reduced to a circular segment, and a periodicity condition was applied—Figure 3. This is also possible because both discs operate with a vortex casing at the outlet. As it was investigated by the author, the flow structure between the discs is independent of the geometry of the vortex casing. Therefore, for computational purposes, the channel was excluded from the analysis.

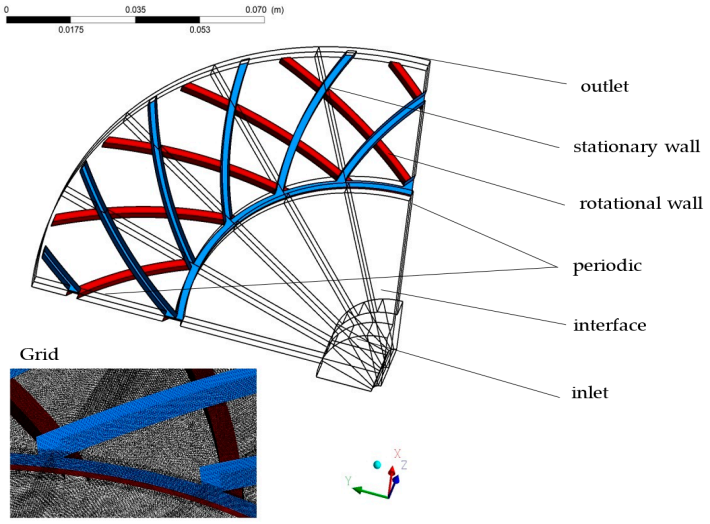


Figure 3. Computational model.

Three-dimensional solid models of the flow section for each geometric variant were created using CATIA v5 software. The discretization of these models was performed using an ANSYS ICEM R2021 R1. The software facilitated the creation of structured meshes for all the models utilizing hexahedral elements. The number of elements in the numerical mesh depended on the specific case under analysis and ranged within $z_{CFD} \in \langle 45–60 \rangle$ million

elements (alteration of the angle of the crucial segment). The boundary layer was discretized using multilevel hexahedral elements, with the number of layers customized individually for each model. The clearance was assumed to be δ_{cb} = 0.6 mm, and the number of grid levels within the clearance was set to 30. The parameters of the mesh for model *zl1* are presented in Table 2.

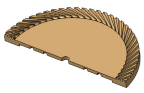
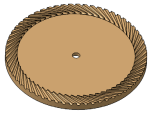
Table 2. Parameters of the computational meshes.

Element	Number of Nodes	Number of Elements	Quality (ICEM)	Skew, °
Inlet pipe	152,822	146,880	0.7	>58
Active disc	2,073,823	1,977,864	0.4	>46
Passive disc	1,516,104	1,919,363	0.45	>42

Numerical flow analysis was performed using the MRF model (multiple reference frames). Simulations were carried out as transient analyses under specified boundary conditions—Figure 3. As a solver, Ansys Fluent CFD was chosen. The analysis was carried out for an active disc rotation speed of n = 3000 rpm. The fluid was pure water with a density of ρ_{H2O} = 998.2 kg and a dynamic viscosity of μ_{H2O} = 0.001003 Pa·s.

An analysis was conducted to evaluate the impact of using a simplified geometric model that assumes periodic flow symmetry. The relative number of mesh elements and other mesh properties remained identical to those presented above. The results of the testes are presented in Table 3. These data represent the relationship between the number of segments corresponding to the head. Data indicate that a minimum of 3 segments are required to achieve stable simulation results, as head values stabilize around 22.3–22.4 m, with further increases in the number of segments having negligible impact.

Table 3. Simulation results for different numbers of segments.

Number of Segments	Head, m	Angle, °	View
1	21.2	12	
2	22.1	24	
3	22.4	36	
4	22.4	48	
7	22.3	84	
15	22.2	180	
30	22.3	360	

The flow modeling in the radial labyrinth pump was performed using the two-equation k–ε realizable turbulence mode. The other turbulence models were tested. In the

table below, Table 4 shows the simulation results for different turbulence models for the *zk13* model (analyzed by the authors in [50]).

Table 4. Simulation results for different turbulence models.

Element	Deviation in Head (%)
Standard	22.1
k–ε Realizable	3.0
k–ε RNG	7.4
k–ω Standard	13.1
k–ω SST	6.3
Reynolds Stress Model	19.6

When evaluating the parameters in BEP, the greatest deviation from the experimental data occurred in the *k*–ε turbulence model, where the discrepancy reached approximately 22.1% of the experimentally measured head. For *k*–ε, the RNG model reduced this difference to just 7.4%. The most accurate results were achieved with unstable simulations, showing just a 3.0% discrepancy for the *k*–ε realizable turbulence model. For model *k*–ω, the standard the deviation is equal to 13.1%, *k*–ω SST—6.3% and Reynolds stress model—19.6%.

3.2. Grid Independence Test

A grid independence test is a crucial step in CFD (computational fluid dynamics) studies to ensure that the numerical results are not influenced by the discretization of the computational domain. It involves analyzing the sensitivity of key results, such as the pump head, in this case, to the density of the computational grid. The test was performed for model *zk1* for *n* = 2000 rpm. The results are shown in Figure 4.

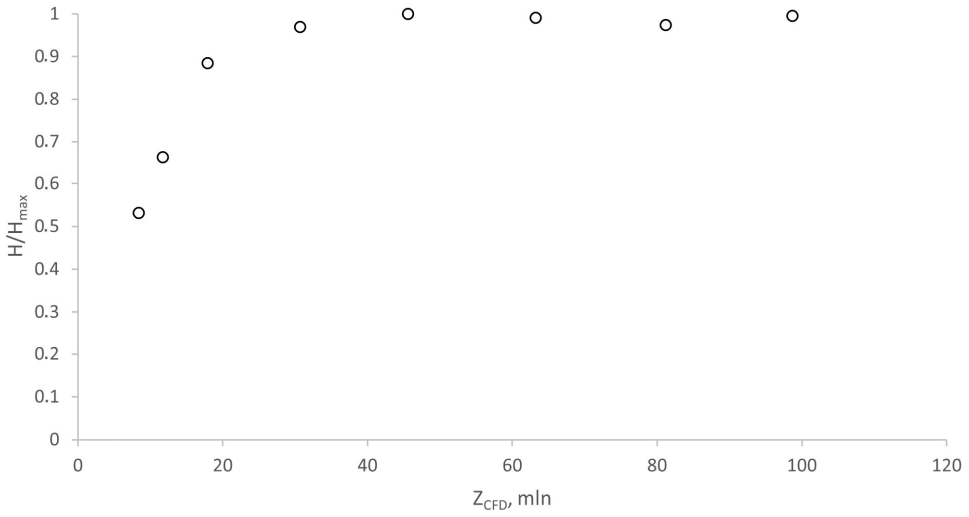


Figure 4. The results of the mesh independence test.

As can be seen in Figure 4, which shows the relationship between the head H relative to the maximum head value H_{max} as a function of the number of computational elements of the grid z_{CFD}, stabilization of the head is observed for grids greater than approximately 40 million elements. Below this value, the head decreases, which may be caused by an incomplete representation of the circulating flow in the pump channels due to the sparse grid.

Since the models differed in the angular segment that defines the periodicity of each case, the number of mesh elements varied between them. However, the mesh density and the discretization approach remained consistent across all models.

3.3. Validation of the Computational Model

Validation of the computational model involved comparing the results of the numerical simulation with the experimental data to evaluate the accuracy and reliability of the model. The primary objective was to ensure that the CFD model could reproduce the performance characteristics of the analyzed pump with an acceptable deviation.

The validation of the model was carried out for two configurations: model *zk13* (analyzed by the authors in [50]) operating with a smooth passive disc and one with a bladed one. This approach was based on the anticipated differences in the mechanisms of energy conversion between the discs and the fluid in the two models, which required verification using CFD methods. The analysis was carried out at a rotational speed of n = 2000 rpm.

Figures 5 and 6 present a comparison of the flow characteristics of an active bladed disc paired with a smooth and bladed passive disc, obtained from experimental measurements and numerical simulation.

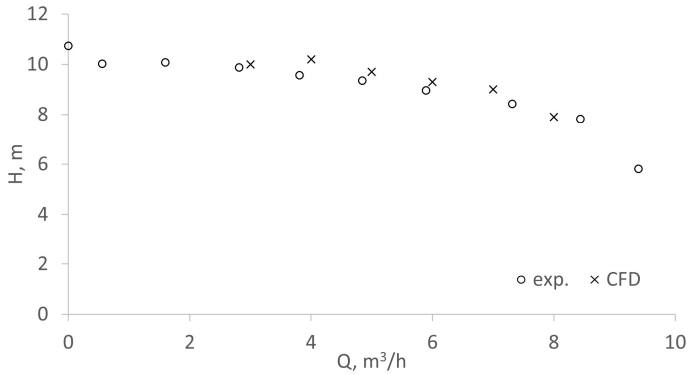


Figure 5. Comparison of the flow characteristics: experimental and CFD results for a bladed active disc and smooth passive disc.

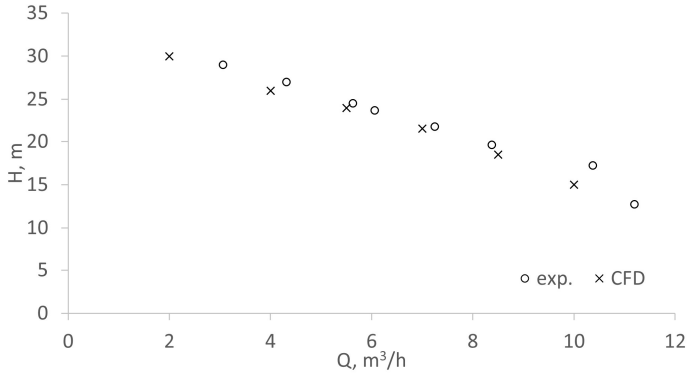


Figure 6. Comparison of the flow characteristics: experimental and CFD results for a bladed active disc and bladed passive disc.

In summary, during the construction of the numerical model, about 21 numerical grids were created, which were used to define the shape and test the model. For further numerical simulations, 5 of them were used.

4. Results and Analysis

4.1. Flow Analysis for an Active Bladed Disc Operating with a Smooth Passive Disc

When analyzing the distribution of the relative velocity vectors within the area of the active disc (model *zl0*, Figure 7, where the blades of the active disc are marked in red), the centrifugal radial flow of the liquid can be observed. The presence of vortices near the

vicinity of the inner diameter d1ap results from the closure of the inlet cross-section of the flow passage.

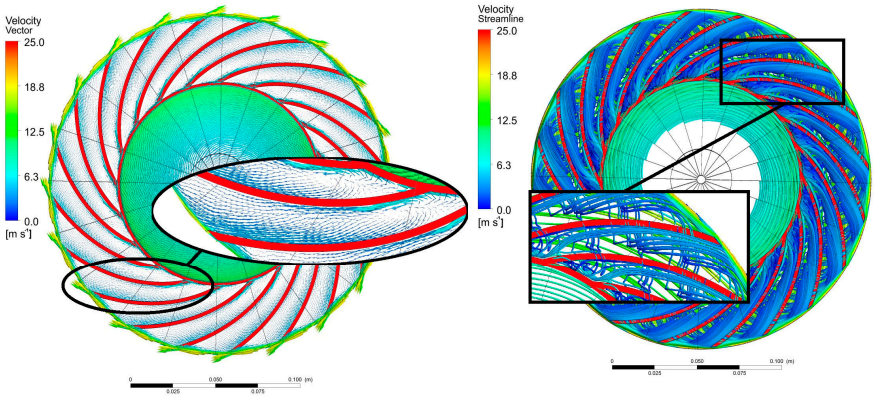


Figure 7. Relative velocity vectors and streamlines (relative) for an active disc with blades and a smooth passive disc, Q = 0.55 m^3/h.

The fluid streamline trajectories depicted in Figure 7 illustrate that, in addition to centrifugal motion, fluid particles follow spiral paths in flow passages. This phenomenon is caused by the interaction of the stationary, smooth passive disc with the fluid located in the flow passages of the rotating active disc.

The fluid in the flow passage is characterized by relative velocity and meets one of the channel walls that remains stationary. Since the velocity on the stationary wall is zero u_p = 0 and the fluid is characterized by a circumferential component of the velocity ua, the difference in velocity ($u_p - u_a$) induces a spiral motion. This spiral effect becomes more pronounced as the difference increases. Spiral movement of the fluid does not contribute to an increase in pump performance. Between the active and passive sides of the blade, there are tip-related volumetric losses caused by the energy difference across the blade. These losses are more significant as the width of the gap width δ between the discs increases. The fluid flow within the gap δ is illustrated in Figure 7.

4.2. Flow Analysis for an Active Bladed Disc Operating with a Bladed Passive Disc

The primary role of the passive disc is to initiate and sustain the momentum exchange process between cooperating working elements. To identify the flow through the set of bladed discs, the set *zk1* described in Table 1 was selected for analysis. This choice was dictated by the highest achieved specific energy value Y_0 (for Q = 0 m^3/h), as well as a 1.7 increase compared to an operation with a smooth passive disc (BEP). For better clarity of the diagrams (Figure 8), the active disc blades are depicted in blue, while the outline of the passive disc blades is marked with black contour lines.

Analyzing Figure 8, which shows the distribution of absolute velocity vectors in the channel between the passive disc blades, it reveals swirling structures that detach from the tips of the active disc blades and pass through the stationary channel of the passive disc. The process of forming these vortices occurs along the entire length of the stationary blade channel, regardless of the position of the active disc blades. These phenomena are also confirmed by the distribution of absolute velocity in the plane located along the flow channels of the passive disc. Analyzing the presented view of absolute velocity isolines in the passive disc channels, numerous areas with reduced velocity are visible, indicating the presence of swirling structures. An important fact is that these areas encompass both the active and passive disc channels and confirm that a transfer of momentum is occurring here.

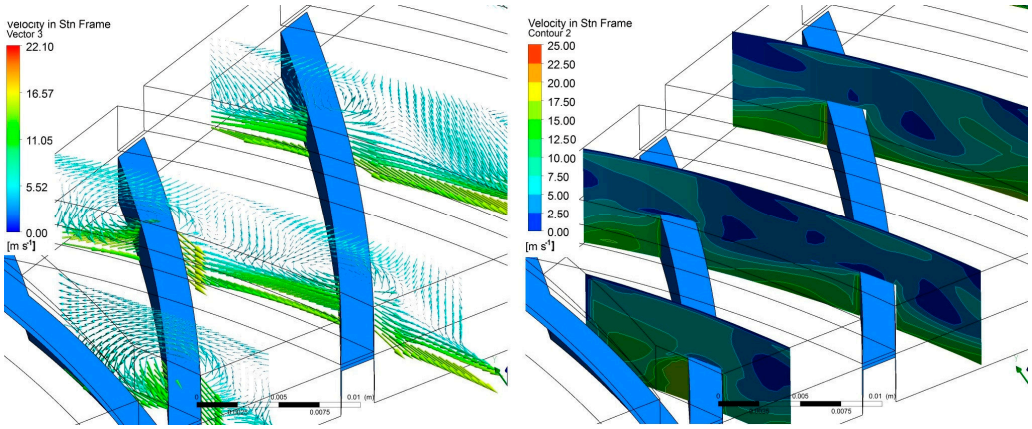


Figure 8. Isolines and velocity vectors (absolute), $Q = 1.37\ m^3/h$.

Since pump operation involves continuous movement of the active disc blades along the passive disc flow passages, this vortex generation phenomenon also takes on a continuous nature.

Because the numerical simulations were conducted as transient and covered the entire length of the flow passage of the passive disc, it is possible to trace the behavior of the pump studied over time. The phenomena that occur in the pump for a flow rate $Q = 0.55\ m^3/h$ and for a time range from $t = 0.00015$ s to $t = 0.0009$ s are shown in Figures 9–14. The presented distributions demonstrate that, throughout the entire range of active disc blades position changes, vortex structures are formed. The nature of this process is continuous, which means that the moving blade, relative to the stationary channel of the passive disc, generates a vortex that detaches from the blade tip. It forms at the entrance to the passive disc channel, moves along the channel, and disappears at the end. The liquid particles forming vortices that detach from the active blade pass through the flow channels of the passive disc and then flow back into the flow channel of the active disc, repeating the vortex generation process. As a result, the liquid flows repeatedly between the active and passive discs.

The structures of the vortex that form are illustrated in Figure 15, which shows the fluid troughs in the channels of the passive disc. Analyzing the presented diagram (with the enlargement detail) confirms the generation of vortices from the tips of the active disc blades, the outline of which are clearly visible based on their distribution.

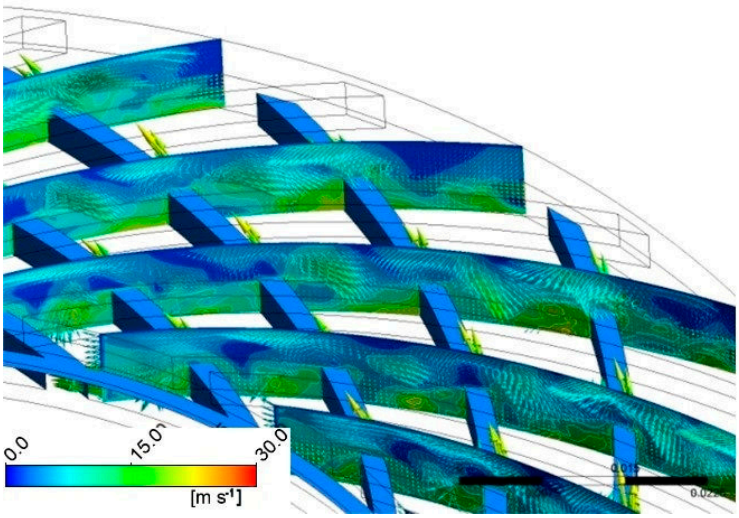


Figure 9. Isolines and velocity vectors (absolute) at $t = 0.00015$ s, $Q = 0.55\ m^3/h$.

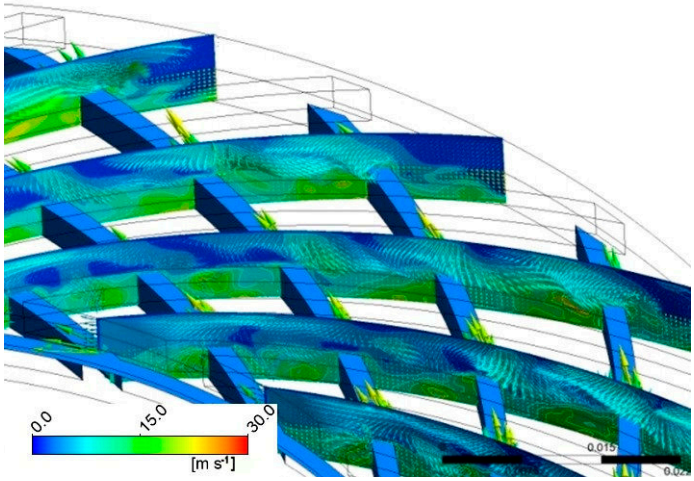


Figure 10. Isolines and velocity vectors (absolute) at t = 0.0003 s, Q = 0.55 m^3/h.

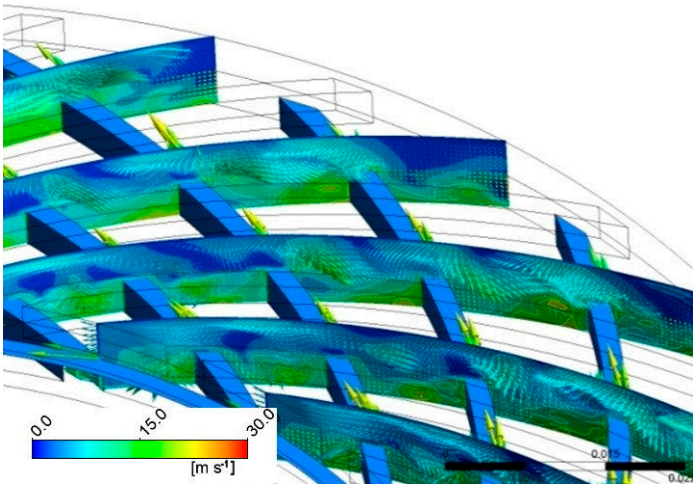


Figure 11. Isolines and velocity vectors (absolute) at t = 0.00054 s, Q = 0.55 m^3/h.

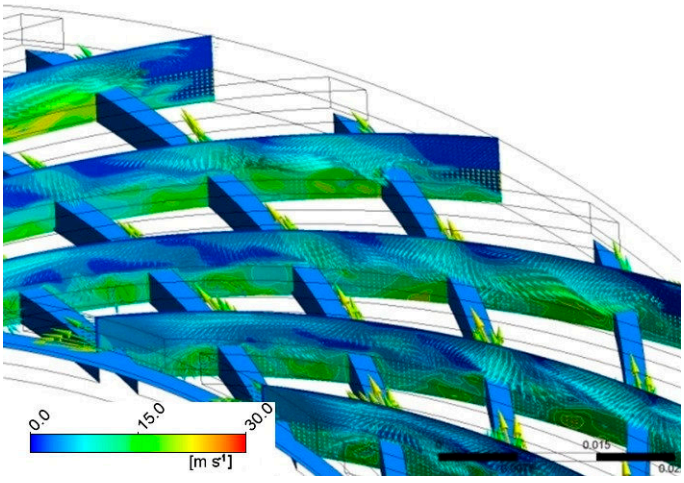


Figure 12. Isolines and velocity vectors (absolute) at t = 0.0006 s, Q = 0.55 m^3/h.

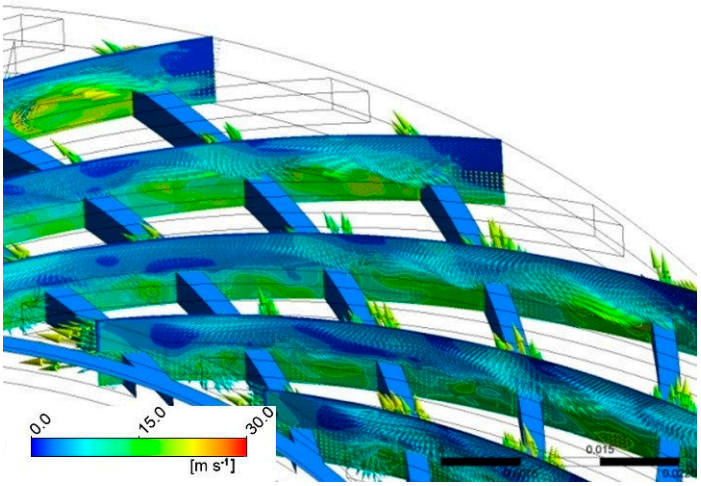


Figure 13. Isolines and velocity vectors (absolute) at t = 0.00075 s, Q = 0.55 m^3/h.

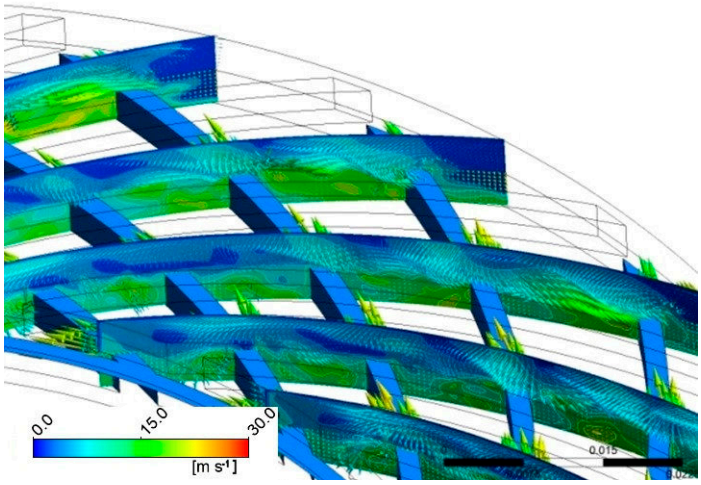


Figure 14. Isolines and velocity vectors (absolute) at t = 0.0009 s, Q = 0.55 m^3/h.

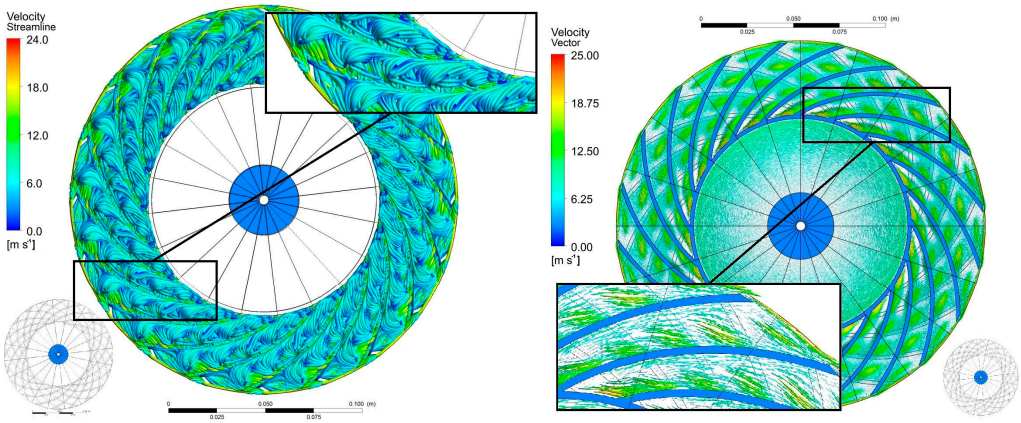


Figure 15. Streamlines (relative) and velocity vectors within the working elements for a passive disc equipped with blades at Q = 1.37 m^3/h.

Similarly to the disc set *zl0* working with the smooth passive disc, the examined disc set *zl1* also exhibits centrifugal energy transfer to the fluid. This process is depicted by the relative velocity vectors shown in Figure 15. In the zoomed view, the flow structure is similar to that of centrifugal pumps with a low specific speed nq being visible. Areas

with higher velocity (colored green–yellow) correspond to locations where the fluid moves from the passive disc to the active disc. A notable feature is that there is a visible effect indicating that energy is being added to the fluid due to the momentum exchange (in each cell formed by the intersecting blades of both discs).

The vortices move along the channels of the passive disc, near the inner edge of the blades, as a result of the rotational motion of the active disc. These phenomena occur for the set analyzed throughout the range of the flow rate Q studied, as shown in Figures 16–19. The diagrams present distributions of absolute velocity and relative streamlines.

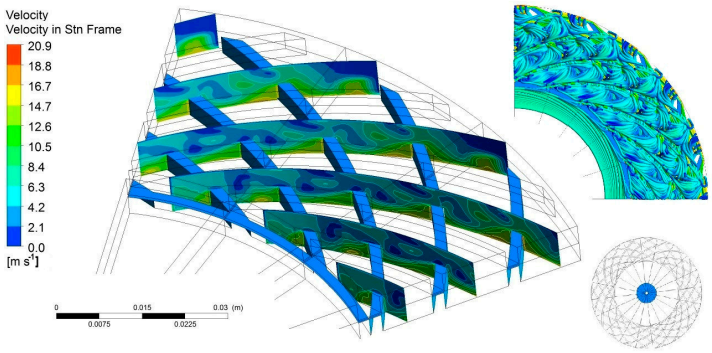


Figure 16. Isolines of velocity (absolute) and particle trajectories (relative) at Q = 0.55 m^3/h.

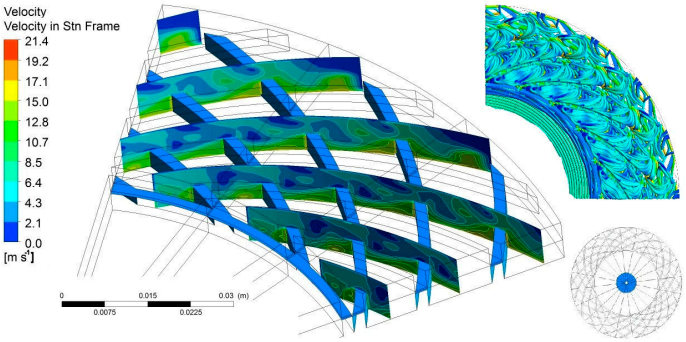


Figure 17. Isolines of velocity (absolute) and particle trajectories (relative) at Q = 2.75 m^3/h.

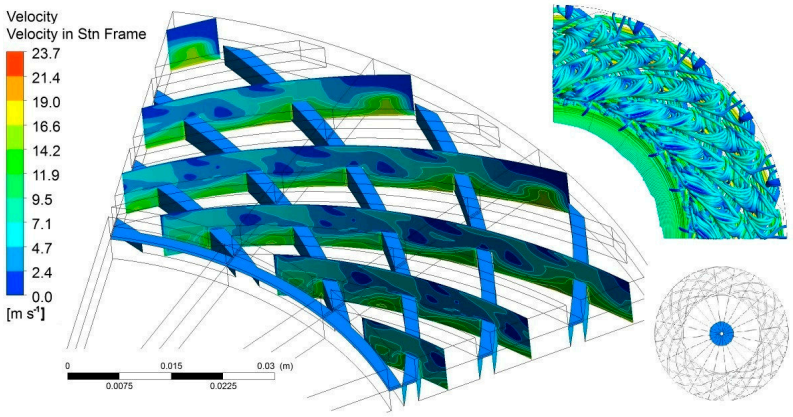


Figure 18. Isolines of velocity (absolute) and particle trajectories (relative) at Q = 5.50 m^3/h.

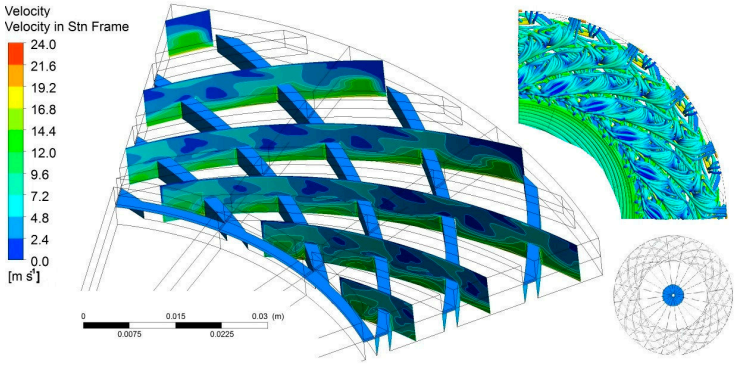


Figure 19. Isolines of velocity (absolute) and particle trajectories (relative) at Q = 8.24 m^3/h.

The averaged flow direction of the liquid in the stationary channel is opposite to the flow generated by the pump, as indicated by the directions and orientations of the velocity vectors shown in Figure 8. However, it should be noted that the role of the passive disc is not to transport the fluid but to increase its energy through the transfer of momentum.As presented in the above considerations, the working process in the analyzed set of bladed discs is a superposition of the centrifugal effect of the active disc on the fluid and the process of vortex detachment from the blade edges of the active disc, which leads to momentum transfer.

4.3. Flow Analysis for an Active Bladed Disc Operating with Passive Blades with Narrow Passages

To identify the flow through the set of bladed discs with narrow passages and wide blades, the set *zl2* described in Table 1 was selected for analysis. Figure 20 shows the streamlines within the active disc (relative) and the passive disc (absolute).

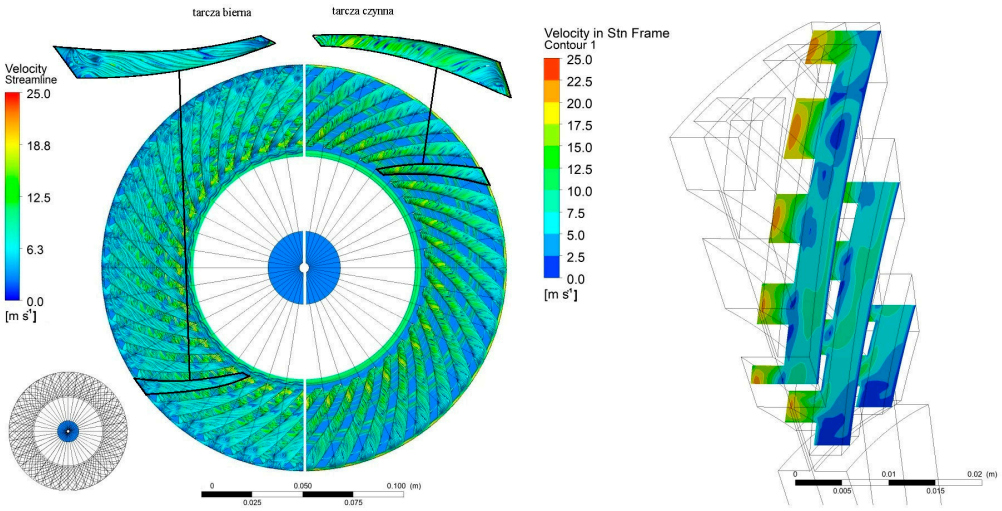


Figure 20. Particle trajectories within the active disc (relative) and passive disc (absolute), also isolines, Q = 0.55 m^3/h.

In the flow channels of the active disc, there is a centrifugal flow of the fluid from the inlet to the outlet. The fluid particles follow a spiral path along the channel, similar to the active disc working with a smooth passive disc. Taking into account the shape of the streamlines in the passages of the passive disc, the flow pattern is analogous: the fluid moves in a spiral motion, induced by the rotating active disc. However, the direction of this flow is the opposite, backwards. The active disc increases the swirling of the fluid, while the channels of the passive disc allow the equalization of energy, leading to increased volumetric losses compared to cooperation with a smooth passive disc. As a result, this causes a reduction in the pump head H.

In contrast to the previous set *zl1*, no vortex structures are formed, which would typically originate from the tip of the active disc blade. Analyzing Figure 20, which shows the absolute velocity isolines in the flow channel of the passive disc, there is a clear absence of areas with reduced velocity that would extend into the flow channel of the active disc. It could be concluded that, in the analyzed case, there is no momentum exchange between the two elements, which was also confirmed by the distribution of the velocity vectors. The results of unsteady simulations for different flow rate values Q show identical phenomena as described above. The presented analysis leads to the conclusion that the absence of vortex formation is caused by the too-narrow flow channel and the excessive thickness of the blades.

Due to the divergent nature of the flow passages of both discs, depending on the appropriate geometric relationships, a situation may arise where the inner part of both discs will cooperate similarly to the one mentioned above, while the outer part will behave as for set *zk1*. In this case, the studied set will be characterized by a higher H when it cooperates with the bladed passive disc. Examples of such geometric parameter configuration describing the shape of the discs is *zl3*, presented in Table 1. Figure 21 shows the absolute streamlines in the flow passages of the passive disc.

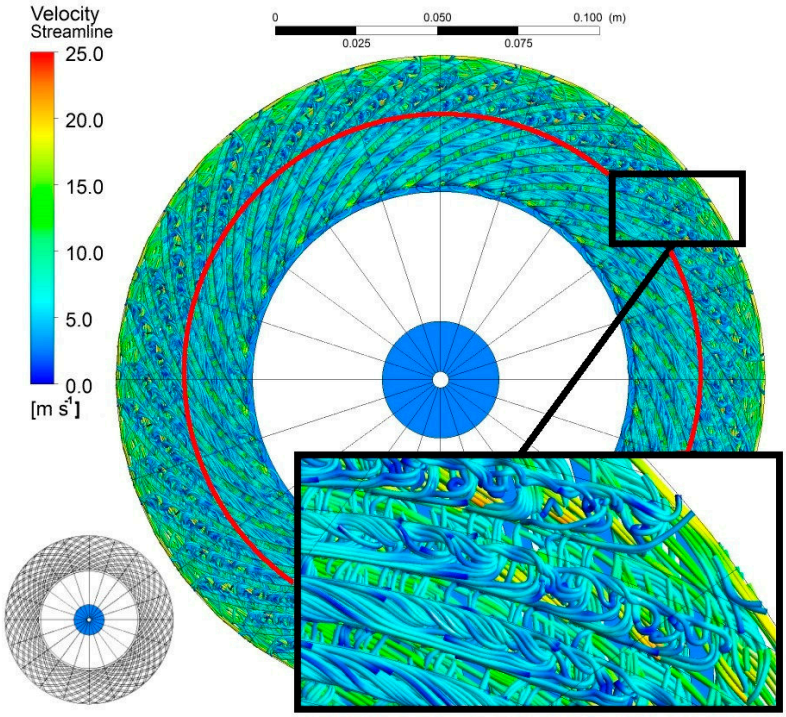


Figure 21. Isolines and velocity vectors (absolute) at Q = 1.37 m^3/h.

When the results of the numerical simulations are analyzed, two working zones of the discs can be identified. Both zones separate the way where the energy is exchanged; as expected, for the inner zone, it is centrifugal, while, in the outer vortex, structures begin to appear, exchanging momentum between the two elements (the red line in Figure 21 marks the boundary of these zones). The analyzed set achieved a higher head H for the passive bladed disc configuration with the bladed passive disc compared to a smooth one—H = 37.5% (Q = 0.55 m^3/h). This increase can be explained by the dominant nature of the momentum exchange, as it occurs at a larger diameter of the disc (Figure 22).

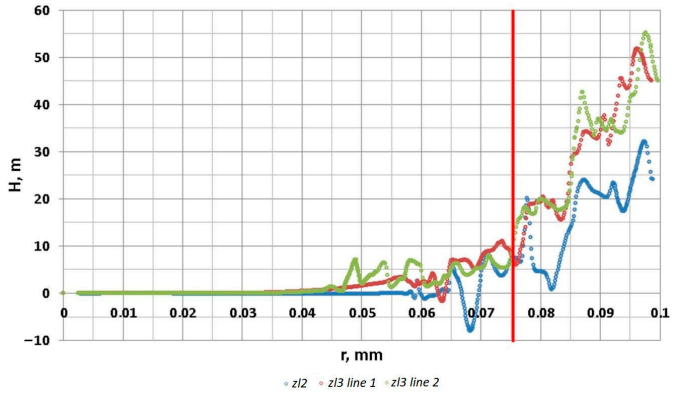


Figure 22. The dependence of the head H as a function of the radius r in the analyzed sets at a flow rate of Q = 0.55 m^3/h.

4.4. Flow Analysis for an Active Blade Disc Operating with a Passive Blade Disc—Short Flow Channel with a Narrow Blade

To identify the flow through the set of bladed discs with a short flow channel with a narrow blade, the set *zl4* described in Table 1 was selected for analysis. Figure 23 shows the relative streamlines in the working elements of the set examined. Similarly to the previous sets, the fluid passing through the active disc undergoes an increase in angular momentum. Due to the geometric shape of the flow channels in both discs, their arrangement does not allow for the formation of a sufficient number of cells (bounded by the blades). In the most favorable position for the case studied, there is only one cell per flow channel, which does not create the conditions necessary for the formation and development of vortex structures.

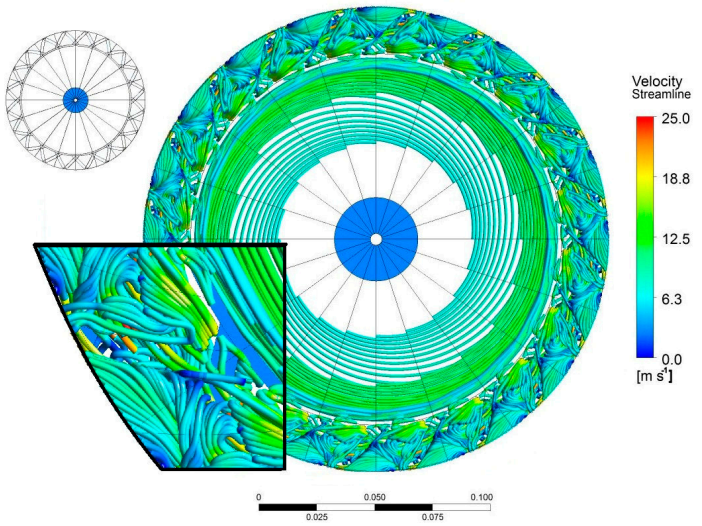


Figure 23. Streamlines (relative) within the active and passive discs at Q = 1.37 m^3/h.

The flow through the passive disc is opposite to the main flow direction through the pump, leading to an increased volumetric loss. Additionally, the wide flow channel of the passive disc does not align with the direction of the absolute velocity of the fluid within the active disc. As a result, the fluid flowing through the passive disc channel strikes the blade and changes the flow direction, which further contributes to the generation of losses in the pump. This phenomenon is depicted in Figure 24, which shows the absolute velocity vectors in the passive disc channel. The velocity isolines exhibit significant variation, which is the cause of the described phenomena but is not related to the momentum exchange between the two discs. The analysis presented leads to the conclusion that the absence of

vortex formation in the second subgroup sets is due to the too-wide and the insufficient number of cells formed by the blades of both discs.

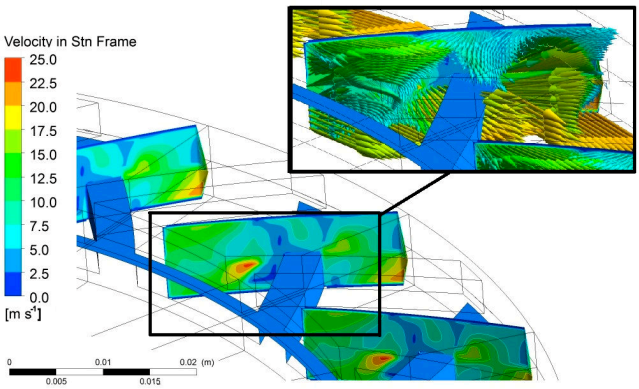


Figure 24. Isolines and velocity vectors (absolute) at Q = 1.37 m^3/h.

4.5. The Quantitative Analysis of the Investigated Models

The quantitative analysis of the analyzed models is provided in Table 5.

Table 5. Quantitative analysis of the investigated models.

Symbol	Head Q = 4.12 m^3/h	Est. Head Q = 0 m^3/h
	H (m)	H_0 (m)
zl0	18.2	24.1
zl1	49.0	40.3
zl2	19.7	24.3
zl3	35.6	48.1
zl4	9.8	14.2

The table presents the head performance data of different models under two flow conditions: head at Q = 4.12 m^3/h and estimated head at Q = 0 m^3/h (H_0), representing the shut off head condition. The model *zl0* achieves a head of 18.2 m at Q = 4.12 m^3/h and 24.1 m at Q = 0 m^3/h. Model *zl1* exhibits a significantly higher performance, with a head of 49.0 m at Q = 4.12 m^3/h and 40.3 m at Q = 0 m^3/h. The model *zl2* performs similarly to *zl0*, with 19.7 m at Q = 4.12 m^3/h and 24.3 m at Q = 0 m^3/h. The model *zl3* demonstrates a moderate performance, achieving 35.6 m at Q = 4.12 m^3/h and 48.1 m at Q = 0 m^3/h. Finally, model *zl4* shows the lowest performance, with a head of 9.8 m at Q = 4.12 m^3/h and 14.2 m at Q = 0 m^3/h. These data illustrate the variation in head performance among the analyzed models, likely influenced by differences in their geometry or operational characteristics, which were described in the sections above.

The flow curves obtained during the investigations are presented in Figure 25.

By analyzing the presented chart, the conclusions from the qualitative flow analysis can be confirmed. The data reveal the following trends:

- *zl1* exhibits the highest head values across flow rates, starting above 50 m at a low flow and gradually decreasing as the flow rate increases. The curve is unsteady. The F-type curve was obtained.
- *zl3* shows moderate head values, consistently higher than the other models, except *zl1*, ranging between approximately 35 m and 45 m.
- *zl0* and *zl2* show similar trends, maintaining head values between 20 and 25 m in the flow range. These models are characterized by low-momentum exchange. As shown in the previous section, it is almost nonexistent here.

- *zl4* demonstrates the lowest head performance, starting below 15 m and slightly decreasing as the flow rate increases.

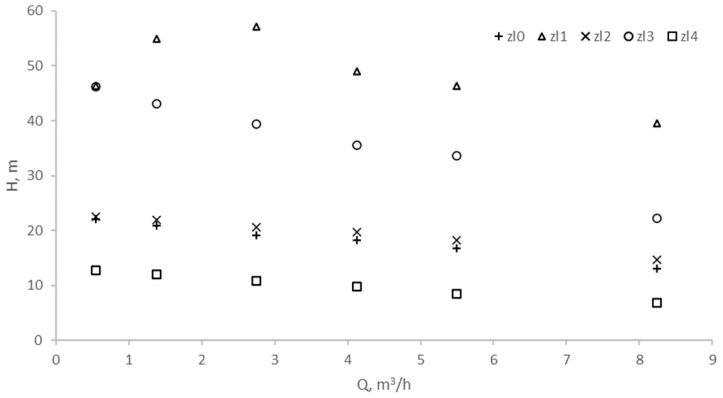


Figure 25. Comparison of flow curves for the analyzed models.

The quantitative results obtained align with the qualitative descriptions of the phenomena. Geometries that promote increased momentum exchange achieve significantly higher head values.

5. Summary

Radial labyrinth machinery (operating as pumps) is a device with a relatively unexplored working process and hydraulic potential. The experimental studies and numerical simulations conducted have expanded our knowledge about the operation of discs equipped with channels and blades. The research findings provided not only specific insights into the impact of the selected geometric parameters of the pump's working elements on its performance but also facilitated, through CFD simulations, the identification of the energy exchange process.

During the research conducted, it was identified that it is beneficial to use discs where the working elements are equipped with blades. The thickness and height of these blades, relative to the width of the flow channel, enable the formation of vortex structures at the tips of the active disc blades, which interact with the passive part of the device. In the case of thick blades with low height and narrow flow channels (e.g., configuration *zl2*), this energy exchange process does not occur. In this configuration, the active disc exerts a centrifugal force on the fluid, while the passive disc, through backflow, increases volumetric losses, leading to a reduction in the head H.

An important factor is the number of cells limited by the blades on both discs, which cannot be maximized, as in the case of an axial labyrinth pump. The use of a large number of cells (e.g., *zl2*) with thick blades and a small number of cells with narrow blades (e.g., *zl4*) relative to the width of the flow channel does not lead to an increase in the head H. The application of narrow blades causes vortices separation from the active disc, but the small number of cells prevents the momentum exchange process and the increase in head H; the passive disc, through backflow, negatively impacts the hydraulic parameters.

For discs equipped with blades of constant cross-section, as the radius of the discs increases, the width of the flow channel also increases. This results in each group of cells along a given circumference being characterized by a different flow area, so they may operate differently. In the case of discs with a large number of blades and large angles, the inner portion of the blades operates centrifugally. However, as the width of the flow passage increases, vortex structures that support momentum exchange may begin to form. The research conducted does not fully describe the issue of the operation of a radial labyrinth pump.

The possibility of using active disc blades with sharpened edges should be considered, as this would undoubtedly influence the pump work process. The geometric identity of both discs presented in this study, driven by the need to reduce the geometric variables,

may not lead to an optimal solution. Therefore, the use of two different discs should be considered, and this aspect should be the subject of further research.

The studied disc sets, in addition to their application as pumping units, could also be used as a non-contact sealing element for rotating parts in machinery. Due to the lack of sealing at n = 0 rpm, the design should be equipped with an additional sealing system to prevent fluid leakage when the machine is idle. Furthermore, the set can be applied as a mixing device for liquids that are difficult to blend while also enabling their pumping. Additionally, the phenomenon of cavitation can intensify the mixing process by cavitation-driven interaction between the two fluids.

Author Contributions: Conceptualization, P.S.; methodology, P.S.; software, J.S.; formal analysis, P.S.; investigation, P.S.; resources, J.S.; data curation, P.S.; writing—original draft, P.S.; writing—review and editing, J.S. All authors have read and agreed to the published version of the manuscript.

Funding: This research was funded by the internal research funds of the Department of Energy Conversion Engineering at Wroclaw University of Science and Technology, Poland, No. 8211104160.

Data Availability Statement: The data presented in this study are available on request from the corresponding author.

Conflicts of Interest: The authors declare no conflicts of interest.

Nomenclature

d	Diameter (mm)
d_{1ap}	Inlet diameter of active/passive disc (mm)
d_{2ap}	Outlet diameter of active/passive disc (mm)
h	Height (mm)
H	Pump total head (m)
k	Head coefficient (for labyrinth pump)
n	Rotational speed (rpm)
n_q	Kinematic specific speed ($n_q = nQ^{0.5}/H^{0.75}$) (rpm)
s	Width (mm)
t	Time (s)
u	Circumferential velocity (m/s)
Q	Flow rate (m^3/s)
Y_0	Specific energy (J/kg)
z	Number of blades
z_{CFD}	Number of grid cells
β	Blades angle (°)
δ	Clearance (mm)
μ	Viscosity (Pa·s)

References

1. Satoh, H.; Uchida, K.; Cao, Y. Designing an Ultra–Low Specific Speed Centrifugal Pump. *Turbomachinery* **2005**, *33*, 316–322.
2. Adler, D. Low Specific Speed Impeller. Patent 96/08655, 21 March 1996.
3. Koji, K. Low Specific Speed Impeller. Patent 7208392 A, 1994.
4. Koji, K. Low Specific Speed Impeller. Patent 9209983 A, 1997.
5. Hergt, P.; Nivklas, A.; Scianna, S. Centrifugal Pump Impeller with Low Specific Speed. Patent 90/07650, 1990.
6. Gulich, J. *Centrifugal Pumps*; Springer: Berlin/Heidelberg, Germany, 2020.
7. Jedral, W. *Rotodynamic Pumps*; PWN: Warsaw, Poland, 2014.
8. Meng, Y.; Li, C.; Yan, H.; Liu, X. Numerical simulation of the ultra–high–speed lowspecific–speed rotodynamic pump and application research in hydraulic system. In Proceedings of the IPCSIT, Singapore, 16–18 September 2011; Volume 2, pp. 179–183.
9. Kurokawa, J.; Yamada, T.; Hiraga, H. Performance of low specific speed pumps. In Proceedings of the 11th Australasian Fluid Mechanics Conference, Hobart, Australia, 14–18 December 1992; pp. 861–864.
10. Skrzypacz, J. Investigating the impact of multi–piped impellers design on the efficiency of rotodynamic pumps operating at ultra–low specific speed. *Chem. Eng. Process.* **2014**, *86*, 145–152. [CrossRef]
11. Golubiev, A.I. Labirynth Pump. Patent USSR 602029/25, 1960.
12. Golubev, A.I. *Labityntn Pumps for Chemical Purposes*; Mashgiz: Moscow, Russia, 1961.

13. Golubev, A.I. *Labityntn–Threaded Pumps and Sealings for Aggressive Fluids*; Mashynostroyene: Moscow, Russia, 1981.
14. Golubev, A.I.; Pyatigorskaya, E.I. Efficiency coefficients of a labyrinth pump. *Chem. Pet. Eng.* **2005**, *41*, 260–266. [CrossRef]
15. Grabow, G. Vergleichsbetrachtungen zu Seitenkanal–, Labyrinth– und Strahlpumpen. *Forsch. Im Ingenieurwesen–Eng. Res.* **1994**, *62*, 11–20. [CrossRef]
16. Golubev, A.I.; Pyatigorskaya, E.I. Determination of optimal parameters of labyrinth–screw seals and pump. In Proceedings of the 16th International Conference on Fluid Sealing, Brugge, Belgium, 18–20 September 2000.
17. Golubev, A.I.; Pyatigorskaya, E.I. Optimization of the hydraulic calculation for labyrinth–screw seals and pumps. In Proceedings of the Ninth International Scientific–Technical Conference Hervicon–99, Sumy, Ukraine, 7–10 September 1999.
18. Guo, Y. Numerical and Experimental Simulation of the Trapezii Form Labyrinth Screw Pump. Ph.D. Dissertation, Beijing University of Chemical Technology, Beijing, China, 2005.
19. Guo, Y.; Zhang, Y.; Li, J. Numerical simulation of the interial flow in a complex trapeziform labyrinth screw pump. *J. Beijing Univ. Chem. Technol.* **2008**, *35*, 44–49.
20. Ma, R. CFD Numerical Simulation and Experimental Study of the Pumping Mechanism and Pumping Performance of Labyrinth Screw Pump. Ph.D. Dissertation, Beijing University of Chemical Technology, Beijing, China, 2009.
21. Ma, R.; Wang, K. CFD Numerical simulation and experimental study of effects of screw–sleeve fitting clearance upon triangular thread labyrinth screw pump. *J. Appl. Fluid Mech.* **2010**, *3*, 75–81. [CrossRef]
22. Ma, R.; Wang, K. Modelling of pumping performance of labyrinth screw pump (LSP) by 2d Reynolds stress equation. *J. Fluid Eng.* **2009**, *131*, 085001. [CrossRef]
23. Ma, R.; Wang, K.; Li, J. Study on pumping mechanism of labyrinth screw pump by numerical simulation of computational fluid dynamic (CFD) and pump performance experiment. *Lubr. Eng.* **2008**, *24*, 75–79.
24. Wang, C.; Zhang, H.; Peng, N.; Zhao, B.; Zheng, H. Numerical calculation and experimental study for interior flow field in triangular labyrinth screw pump. *J. Drain. Irrig. Mach. Eng.* **2009**, *27*, 73–77.
25. Zahng, Y.; Yang, C.; Li, J. Numerical simulation and experiment of gas–liquid two–phase flow field in labyrinth screw pump. *J. Drain. Irrig. Mach. Eng.* **2010**, *28*, 492–496.
26. Vasilcov, E.A.; Nevelic, V.V. *Hermetic Elektopumps*; Mashynostroenye: Leningrad, Russia, 1968.
27. Andrenk, P.; Lebedev, A. Labyrinth screw pump theory. *Motrol. Comm. Mot. Energetics Agric.* **2014**, *16*, 35–42.
28. Zhang, S.; Zhang, Y.C.; Yan, H.; Yang, W.M. Numerical simulation and experimental study of gas–liquid two–phase flow of series–connected combined labyrinth screw pump. *Ind. Saf. Environ. Prot.* **2016**, *42*, 14–17.
29. Li, J.J.; Zhang, Y.C. Numerical simulation of series combined labyrinth screw pump based on Fluent. *J. Drain. Irrig. Mach. Eng.* **2014**, *32*, 296–301.
30. Ma, Q.Y.; Zhang, Q.Z.; Zhang, L.F.; Silan, F. Numerical simulation and experimental research on the internal flow field of rectangular labyrinth pump. *Fluid Mach.* **2017**, *45*, 1–4.
31. Wang, C.; Zhang, Y.C.; Li, J.Z. CFD simulation of maze screw pump coal water slurry transportation and preliminary discussion of internal wear. *Guangdong Chem. Ind.* **2011**, *38*, 57–59.
32. Rong, X.; Zhu, H.; Hu, B. Performance Research and Structure Optimization of Labyrinth Screw Pump. *Micromachines* **2021**, *12*, 790. [CrossRef]
33. Andrenko, P.; Rogovyi, A.; Hrechka, I.; Khovanskyi, S.; Svynarenko, M. Characteristics improvement of labyrinth screw pumpusing design modification in screw. *J. Phys. Conf. Ser.* **2021**, *1741*, 012024. [CrossRef]
34. Lebedev, A.Y.; Andrenko, P.M.; Grigoriev, A.L. Dynamic analysis of the mechanical seals of the rotor of the labyrinth screw pump. *IOP Conf. Ser. Mater. Sci. Eng.* **2017**, *233*, 012035. [CrossRef]
35. Han, L.; Wang, Y.; Liu, K.; Ban, Z.; Qin, B.; Liu, H.; Dai, M. Theoretical Leakage Equations Towards Liquid–Phase Flow in the Straight–Through Labyrinth Seal. *J. Tribol.* **2021**, *144*, 031802. [CrossRef]
36. Liu, K.; Han, L.; Wang, Y.; Liu, H.; Zhao, D.; Li, X.; Jiang, S. Theoretical and experimental research towards labyrinth sealing mechanism of liquid nitrogen in the cryogenic spindle. *Mech. Syst. Signal Process.* **2022**, *167*, 108502. [CrossRef]
37. Stoff, H. Incompressible flow in a labyrinth seal. *J. Fluid Mech.* **1980**, *100*, 817–829. [CrossRef]
38. Watson, C.; Untaroiu, A.; Wood, H.G.; Weaver, B.K.; Morgan, N.; Jin, H. Response surface mapping of performance for helical groove seals with incompressible flow. In *Turbo Expo: Power for Land, Sea, and Air*; American Society of Mechanical Engineers: New York, NY, USA, 2016; Volume 49842.
39. Watson, C.; Wood, H.G. Developing an optimal helix angle as a function of pressure for helical Groove seals. In *Fluids Engineering Division Summer Meeting*; American Society of Mechanical Engineers: New York, NY, USA, 2017; Volume 58042, p. V01AT05A020.
40. Watson, C.; Wood, H. Evaluating Configurations of Double Surface Helical Groove Seals Using Computational Fluid Dynamics. In *Turbo Expo: Power for Land, Sea, and Air*; American Society of Mechanical Engineers: New York, NY, USA, 2018; Volume 51012, p. V02CT42A053.
41. Watson, C.; Wood, H. Second stage optimization of helical groove seals using computational fluid dynamics to evaluate the dependency of optimized design on preswirl. In *Fluids Engineering Division Summer Meeting*; American Society of Mechanical Engineers: New York, NY, USA, 2018; Volume 51579, p. V003T12A028.
42. Li, T.T. *Theoretical Design, CFD Numerical Calculation and Experimental Study on Rectangle Labyrinth Screw Pump*; Jiangsu University: Zhenjiang, China, 2007.
43. Jia, F. *Large Eddy Simulation and Experimental Study on Trapezium Labyrinth Screw Pump*; Jiangsu University: Zhenjiang, China, 2013.

44. Woo, S.; Jang, H.; Kwak, H.; Moon, Y.; Kim, C. Leakage analysis of helical grooved pump seal using CFD. *J. Mech. Sci. Technol.* **2020**, *34*, 4183–4191. [CrossRef]
45. Wang, Z.; Zhu, J.; Cao, G.; Zhu, H.; Zhong, R.; Zhu, H. Study on the Labyrinth Screw Pump for Heavy Oil Production. In Proceedings of the SPE Asia Pacific Oil & Gas Conference and Exhibition, Adelaide, Australia, 17–19 October 2022.
46. Ke, W.; Zeng, H.; Wang, Z.; Yu, H.; Liu, Y.; Zheng, D.; Zhu, J.; Zhu, H. A Numerical Study on Labyrinth Screw Pump (LSP) Performance under Viscous Fluid Flow. *Energies* **2023**, *16*, 5997. [CrossRef]
47. Guo, X.; Yang, M.; Li, F.; Zhu, Z.; Cui, B. Investigation on Cryogenic Cavitation Characteristics of an Inducer Considering Thermodynamic Effects. *Energies* **2024**, *17*, 3627. [CrossRef]
48. Lin, X.; Zhang, B.; Zhang, M.; Zhao, Y.; Lai, T.; Chen, L.; Xue, R. Influence of Internal Flow on the Performance of High-Speed Centrifugal Pumps with a Fully Sealed Structure. *Appl. Sci.* **2022**, *12*, 5263. [CrossRef]
49. Tan, Y.; Ni, Y.; Xu, W.; Xie, Y.; Li, L.; Tan, D. Key technologies and development trends of the soft abrasive flow finishing method. *J. Zhejiang Univ. Sci. (Appl. Phys. Eng.)* **2023**, *24*, 1043–1064. [CrossRef]
50. Szulc, P.; Skrzypacz, J.; Lorenz, W. Experimental Study of the Influence of the Geometrical Parameters of the Radial Labyrinth Pump on the Pump's Operating Parameters and Performance. *Energies* **2023**, *16*, 5158. [CrossRef]

Disclaimer/Publisher's Note: The statements, opinions and data contained in all publications are solely those of the individual author(s) and contributor(s) and not of MDPI and/or the editor(s). MDPI and/or the editor(s) disclaim responsibility for any injury to people or property resulting from any ideas, methods, instructions or products referred to in the content.